Laser-induced graphene as a sustainable counter electrode for DSSC enabling flexible self-powered integrated harvesting and storage device for indoor application

Electrochimica Acta 460 (2023) 142614

Contents lists available at ScienceDirect

Electrochimica Acta

journal homepage: www.journals.elsevier.com/electrochimica-acta

Laser-induced graphene as a sustainable counter electrode for DSSC enabling flexible self-powered integrated harvesting and storage device for indoor application

Roberto Speranza [a,b,*], Marco Reina [a,b], Pietro Zaccagnini [a], Alessandro Pedico [a], Andrea Lamberti [a,b]

[a] Politecnico di Torino, Dipartimento di Scienza Applicata e Tecnologia (DISAT), Corso Duca degli Abruzzi, 24, Turin 10129, Italy
[b] Istituto Italiano di Tecnologia, Center for Sustainable Future Technologies, Via Livorno, 60, Turin 10144, Italy

ARTICLE INFO

Keywords:
Laser-induced graphene
Supercapacitors
Dye-sensitized solar cells
Energy harvesting
Energy storage
Counter electrode

ABSTRACT

Dye-sensitized solar cells (DSSCs) are gaining a newfound interest thanks to their superior ability to harvest indoor light with efficiency higher than other photovoltaic technologies. This study reports, for the first time, the possibility of using laser-induced graphene (LIG) as a flexible counter electrode material for DSSCs. A flexible LIG (F-LIG) electrode was fabricated by direct laser writing of a polyimide film, without the need of a starting conductive substrate. The prepared electrodes showed a higher catalytic activity towards the reduction of I_3^-/$I^-$with respect to a more expensive Pt-based counter electrode. Moreover, the F-LIG electrodes outperformed electrodeposited PEDOT as a catalytic material for reduction of a copper bipyridyl complex ($Cu^{(II/I)}(tmby)_2TFSI_{2/1}$) electrolyte. The F-LIG based DSSCs showed an open circuit voltage as high as 0.94 V and an increase in photoconversion efficiency higher than 60% with respect to the PEDOT-based counterpart, stepping from 3.08% to 4.96%. Thanks to the easy one-step laser-based fabrication process, the LIG-based DSSC was integrated with a LIG-based supercapacitor (SC), obtaining a flexible energy harvesting and storage system that was able to self-charge both under simulated solar illumination and under indoor artificial illumination, appearing to be a promising energy source for the next generation of self-powered connected Internet of Things devices.

1. Introduction

Right after their invention in 1991, Dye-sensitized solar cells (DSSC) were quickly recognized as a promising photovoltaic (PV) technology. DSSC is characterized by a simple fabrication method that does not require toxic materials and has fewer requirements in the manufacturing process. [1,2]. Moreover DSSC allows design customization, thanks to the possibility of selecting colour, shape and even transparency, both on rigid and flexible substrates [3]. To date, they are still considered the PV technology with one of the lowest pay-back-time [4,5].

Nevertheless, DSSC never actually widely landed on the market, with only few examples connected to aesthetic and building integrated applications [6–8]. This is related to the lower conversion efficiency reached by DSSC with respect to other PV technologies such as silicon solar panels or perovskites solar cells. To date, the highest certified record efficiency is 13%, while one of the highest uncertified value lays at around 14% [9,10].

In the last decade DSSC collected a renewed interest in terms of research activity and large-scale development thanks to the introduction of novel redox mediators based on copper coordination complexes that are enabling unprecedented levels of output voltages, exceeding 1 V for a single cell [11,12]. This complexes, combined with co-sensitizing organic dyes, have allowed novel records of efficiencies under standard AM 1.5 G illumination conditions. Even more notably, efficiencies exceeding 30% have been reported when these DSSC have been characterized under indoor artificial light illumination. [13,14] These new findings open the way to a novel generation of indoor self-powered devices for which a reliable indoor energy source would be a turning point for their large-scale diffusion, solving problems like periodic maintenance, installation limitations and sustainability [15,16]. Moreover, DSSC have been often integrated with supercapacitors (SC) with the goal of providing energy even when the illumination is temporally

* Corresponding author.
E-mail addresses: roberto.speranza@polito.it, roberto.speranza@iit.it (R. Speranza), marco.reina@polito.it, marco.reina@iit.it (M. Reina), pietro.zaccagnini@polito.it (P. Zaccagnini), alessandro.pedico@polito.it (A. Pedico), andrea.lamberti@polito.it, andrea.lamberti@iit.it (A. Lamberti).

https://doi.org/10.1016/j.electacta.2023.142614
Received 30 December 2022; Received in revised form 27 April 2023; Accepted 17 May 2023
Available online 18 May 2023

absent (e.g. at night) [17–19].

Efforts have been made to optimize DSSC building blocks for new redox mediators, with one crucial aspect being the catalytic material used at the counter electrode for reducing the redox couple. [20]. Platinum nanoparticles on a conductive substrate have typically been used with triiodide-iodide (I_3^-/I^-) electrolytes, but Pt is expensive and not as effective with $Cu^{(II/I)}$-based mediators. [21–23] Poly(3, 4-ethylenedioxythiophene) (PEDOT) has been found to be the best counter electrode material for $Cu^{(II/I)}$-based mediators [24,25]. However, the large-scale processability of these electropolymerized PEDOT-based counter electrodes still need to be established.

When flexibility is desired, in most cases both Pt and PEDOT have been deposited on flexible transparent conductive substrates, such as indium tin oxide-coated polyethylene terephthalate (ITO/PET), which is known to have long term stability issues due to possible delamination of the ITO layer following to cracks in the transparent oxide that may arise with time [26].

As an alternative, carbonaceous materials have attracted much attention thanks to their low cost with respect to Pt when processed in large scale. Moreover, carbon-based materials such as graphene or carbon nanotubes proved to be as effective as Pt or PEDOT counter electrodes in combination with I_3^-/I^--based or $Cu^{(II/I)}$-based electrolytes, respectively, with good chemical stability and sometimes even lower resistivity [27,28]. Amongst carbon-based materials for electrochemical systems, laser-induced graphene (LIG) has been widely studied as active material for energy storage devices such as supercapacitors and batteries, sensors and as catalytic element [29–38]. LIG is obtained by direct laser writing of a polymeric surface in which the polymer chains are broken by the energy provided by the laser, with a subsequent reorganization in the form of few-layer graphene nanostructures [39].

LIG has been only remotely studied as a material for solar cells, with only one work that proposed it as an electrode material for heterojunction solar cells [40]. Some reports described the fabrication of DSSC with reduced graphene oxide obtained by laser engraving of graphene oxide layer deposited on conductive substrates [41,42]. To the best of our knowledge, only in one case LIG obtained by polyimide sheets was employed in a DSSC, but in this case the obtained material was mixed with a binder to produce a printable slurry to be coated on a rigid fluorine tin oxide (FTO)-coated glass, therefore losing the advantage of flexibility [43].

Herein we report the fabrication of flexible, low-cost, and highly catalytic LIG counter electrodes for DSSC, compatible both with I_3^-/I^--based and $Cu^{(II/I)}$-based electrolytes. In both cases, we compared the LIG electrodes with the standard materials used as counter electrodes for DSSC, namely Pt and PEDOT, also investigating their mechanical flexibility.

For the fabrication of the flexible LIG electrode, polyimide was used as a starting substrate since it shows a very good mechanical flexibility, it is stable up to 300 °C and it shows a very good chemical resistance. Moreover, it is one of the most common material for the fabrication of LIG electrodes. [30,40,44]

Furthermore, a flexible, self-rechargeable energy storage system was demonstrated using LIG electrodes made through a one-step laser fabrication process. The system combined a DSSC and a SC, with the counter electrode of the DSSC and the two capacitive electrodes of the SC made of LIG. The device could self-charge when exposed to light, with higher storage efficiency in lower illumination intensity, showing the potential, after further development, to be used as an energy source for self-powered indoor devices such as low consuming IoT sensors.

2. Experimental

2.1. Materials

Unless otherwise noted, all the chemicals used in this work were purchased from Sigma-Aldrich and used as received. Fluorine tin oxide (FTO)-coated glass (7 Ω/sq), indium tin oxide coated PET (ITO/PET) (18 Ω/sq), Ruthenizer 535-bisTBA (N719, dye), transparent TiO_2 nanoparticles paste (Ti-Nanoxide T/SP) were purchased from Solaronix. 3-Methoxypropionitrile (MPN), 4-tert-butylpyridine (TBP) and Whatman glass fibre sheets were purchased from Merck. Dye XY1, $Cu^{I}(tmby)_2TFSI$ and $Cu^{II}(tmby)_2TFSI_2$ were purchased from Dyenamo AB. Polyimide (Kapton) foils were purchased from Dupont. Activated carbon YP-50 F was provided by Kuraray and the C65 carbon black was provided by Imerys. Poly(vinylidene fluoride) (PVDF) was provided by Arkema. Fibreglass separators (Whatman, GF/C) were purchased from Sigma-Aldrich.

2.2. LIG electrodes preparation

The LIG electrodes were fabricated according to the procedure reported in a previous work [45]. Briefly, 125 μm thick polyimide (Kapton) foils were exposed to laser radiation using a 30 W CO_2 laser source (EOX 30 W laser by Datalogic). The laser works in pulsed width modulation control and the LIG electrodes were obtained setting a resolution of 400 dpi, a frequency of 4 kHz, a laser velocity of 375 mm s^{-1} and a laser power of 5.7 W.

2.3. DSSC preparation

The photoanodes of the DSSC were prepared as previously reported [18]. Briefly, FTO-coated glass electrodes were cleaned with deionized water, acetone, and ethanol in ultrasonication bath for 15 min. Then, the electrodes were coated with transparent TiO_2 nanoparticles paste by screen printing, dried at 100 °C for 10 min and then sintered for 30 min at 475 °C. For the photoanodes that needed to be used with $Cu^{(II/I)}$-based electrolyte, a previous $TiCl_4$ treatment at 70 °C for 30 min was performed, followed by a sintering process at 475 °C for 30 min, to deposit a nanometric layer of compact TiO_2 that worked as blocking layer, as previously reported [14]. After sintering, the electrodes were immersed into dye solution for 16 h. For the DSSC tested with I_3^-/I^--based electrolyte, a staining solution of 0.3 mM of N719 dye in ethanol was prepared. For the device tested with $Cu^{(II/I)}$-based electrolyte, the staining solution was obtained by 0.1 mM of XY1 dye with 1 mM of chenodeoxycholic acid in isopropanol/ethanol 3:7. After the staining process, the photoanodes were assembled with the counter electrodes with a glass fibre separator filled with the selected electrolyte solution. The I_3^-/I^--based electrolyte was prepared dissolving 0.45 M of NaI, 0.056 M of I_2 and 0.55 M of TBP in MPN. The $Cu^{(II/I)}$-based electrolyte composition was: 0.2 M $Cu^{I}(tmby)_2TFSI$, 0.04 M $Cu^{II}(tmby)_2TFSI_2$, 0.1 lithium bis(trifluoromethanesulfonyl)imide and 0.6 M TBP in MPN.

Finally, the LIG counter electrodes were prepared and directly used as reported in Section 2.2. The active area of the DSSC was 0.7854 cm^2. For the I_3^-/I^--based DSSC, a further treatment was performed on LIG electrodes to increase their active area and electrical conductivity, as reported in our previous work [45]. Briefly, LIG electrodes were infiltrated with a solution of active carbon and carbon black particles, using PVDF as a binder. Untreated and treated LIG electrodes were compared with flexible titanium (Ti) and ITO/PET sheets coated with a nanometric layer of Pt nanoparticles by sputtering technique.

For the $Cu^{(II/I)}$-based DSSC, LIG counter electrodes were compared with flexible ITO/PET sheets coated with PEDOT, prepared with the same procedure reported in the literature by others [24]. The active area of the DSSC was 0.7854 cm^2. For the characterization of the catalytic activity of the selected counter electrodes, dummy cells were prepared by interposing a glass fibre separator filled with electrolyte between two identical counter electrodes. The geometrical active area of the electrodes used for the dummy cell characterization was 0.25 cm^2 for the characterization with the iodine-based electrolyte while it was 0.6 cm^2 for the copper-based electrolyte.

2.4. LIG-based integrated HS system preparation

For the harvesting part of the integrated HS system, a flexible DSSC was fabricated. For the photoanode, the same preparation reported in Section 2.3 was performed, but the rigid FTO-glass was replaced by a flexible Ti mesh with a thickness of 60 μm. The counter electrode of the flexible DSSC as well as the two capacitive electrodes of the flexible supercapacitor were prepared as reported in Section 2.1. A parallel connection between the DSSC and the SC was performed by two shared Ti mesh. A fibreglass separator filled with the appropriate electrolyte was placed in both devices between the electrodes. For the DSSC, the $Cu^{(II/I)}$-based electrolyte prepared as reported in Section 2.3 was used, instead for the SC a 1 M Na_2SO_4 in deionized water was used as electrolyte. The device was sealed in a transparent vacuum sealed pouch bag. The 3D rendering as well as a picture of the prepared device is reported in Fig. 7.

2.5. Characterization

The surface morphology of the prepared electrodes was studied by a field-emission scanning electron microscope (FESEM Zeiss SUPRA40). Electrochemical impedance spectroscopy and linear polarization measurements were performed on symmetrical dummy cells with a Autolab PGSTAT128 potentiostat equipped with an FRA32M module. Cyclic voltammetry measurements were performed on three-electrode cells with a BioLogic VMP3 potentiostat. The same instrument was used to collect the current-voltage (I-V) response of the DSSC. A circular masque with a 3 mm diameter was used to accurately select the illuminated area on the DSSC. A Newport 91195A solar simulator was used to perform the measurements under AM 1.5 G light spectrum, while a LED lamp (12–60 V AC/DC, 10 W, 3000 K, 810 lm from SPL) was used for the measurement under indoor illumination conditions. Finally, the Autolab potentiostat together with a Keithley 2440 source measure unit were used to perform the photo-charge/discharge characterization of the integrated HS device, as previously reported [46].

3. Results and discussion

The main purpose of this work was to demonstrate that LIG can be employed as a cheap, sustainable and easy-to-make counter electrode material for flexible DSSC, allowing at the same time the integration with a supercapacitor sharing one electrode between the two devices and acting both as flexible current collector and as active material.

3.1. Laser-induced graphene as counter electrode for I^-/I_3^--based DSSC

Initially, we decided to establish a common ground with the existing literature. The LIG counter electrodes were tested first in combination with the I_3^-/I^- redox couple, which over the years represented the reference mediator for DSSC together with Pt-coated counter electrodes. Moreover, to relate with the existing literature on flexible counter electrodes for DSSC, we compared flexible LIG (F-LIG) electrode with a Pt-coated titanium foil (Pt-Ti) and with a Pt-coated PET-ITO substrate (Pt-ITO) [47–50].

First the electrocatalytic activity of each material was investigated by electrochemical impedance spectroscopy (EIS) of symmetrical dummy cells. The Nyquist plot of the measurements are reported in Fig. 1a, together with the equivalent circuit used to fit the obtained spectra. In the circuit, R_s modelled the electrode series resistance, R_{ct} represent the charge transfer resistance at the electrode-electrolyte interphase; C_{ct} model the double layer capacitance of the material and the diffusion impedance Z_d model the ion transport diffusion. [51] At first sight, an obvious difference in the overall resistivity of the material was observed, looking at the interception of the impedance spectra with the real axis. As it can be seen, the Pt-Ti dummy cell showed the lower series resistance (R_s) when compared with the other materials, which is

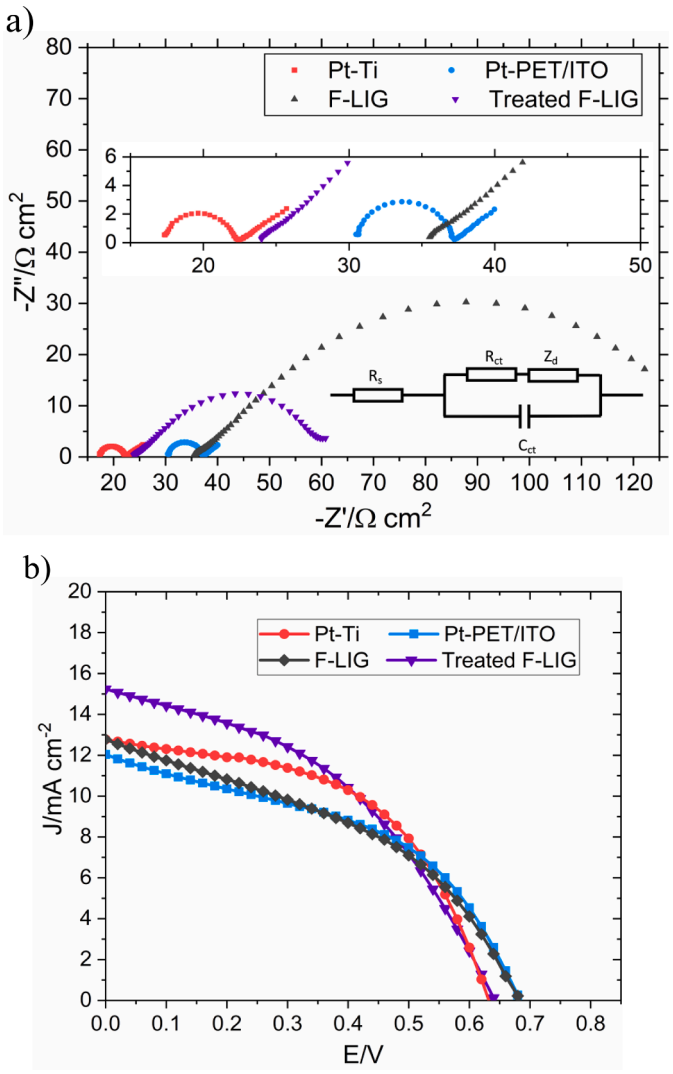

Fig. 1. a) Comparison of EIS measurements of symmetric dummy cell prepared with treated F-LIG, F-LIG, Pt-Ti and Pt-ITO counter electrodes. The insets show the high frequency region of the LIG electrodes and the equivalent circuit used to fit the obtained spectra. b) Comparison of IV characteristic of DSSC fabricated with different counter electrodes.

one of the advantages of having a metallic current collector in the cell. Nevertheless, the use of bulk metallic substrate will inevitably increase the final cost of the device, even more if further treatment such as the Pt-coating is needed. On the other side, both F-LIG and Pt-ITO dummy cells showed a higher value of R_s which will certainly appear when these materials will be employed in full DSSC configuration.

In this regard, it was decided to implement a treatment previously reported in the literature that consisted of decorating the LIG material by vacuum infiltration of particles of active carbon (AC), in order to increase the total surface area, and carbon black (CB) that could improve electrical conductivity. As expected, the effects of this were immediately seen with a substantial reduction in terms of overall R_s, as reported in Table 1.

Further insight regarding the electrocatalytic properties of the tested materials can be extracted from the Nyquist plot looking at the high frequency region of the EIS. Indeed, it is known that the high frequency arc arises from the redox reaction of the I^-/I_3^- mediator happening at the electrode-electrolyte interface and can be modelled with a parallel between a capacitor that account for the double layer capacitance of the material and a charge transfer resistance (R_{ct}) related to the electron transfer at the interfaces [52].

Table 1
Summary of the main parameter extracted from the EIS measurements in symmetrical cell and from the IV characterization of the full DSSC under AM 1.5 G illumination condition.

	EIS dummy cells		DSSC IV characterization			
Counter electrode	R_s (Ω cm^2)	R_{ct} (Ω cm^2)	Jsc (mA cm^{-2})	Voc (V)	FF	η (%)
Pt-Ti	17.2	2.4	12.8	0.63	0.52	4.21
Pt-ITO	30.4	3.2	12.1	0.68	0.46	3.76
F-LIG	35.4	1.3	12.7	0.68	0.41	3.62
Treated F-LIG	23.9	0.5	15.2	0.64	0.43	4.17

Looking at the values of R_{ct} obtained for the different counter electrodes, summarized in Table 1, it is clear how the LIG-based electrodes show a comparable behaviour with respect to the Pt-coated materials. All the electrodes had a R_{ct} far lower than 10 Ω cm^2, which is considered as the limit for good performing DSSC [52]. Moreover, could be evidenced how the treated F-LIG showed the lowest R_{ct} equal to 0.5 Ω cm^2, clearly allowed by the combination of the high surface area of the LIG together with the combination of AC and CB particles which are known to have a positive effect as counter electrode materials for iodine-based DSSC [53,54]. This evidence is in line with other works that showed how carbon and graphene-based porous materials could act as good alternatives to Pt-based counter electrodes for DSSC thanks to their high surface area that allow to drastically increase the actual catalytic surface with respect to the geometrical area [55,56].

Once electrocatalytic activity in combination with the iodine-based electrolyte was tested in dummy cells, the F-LIG counter electrodes, both blank and treated, were characterized in the full DSSC configuration. The photoanode, separator and electrolyte composition were kept the same in all the tested cells. The I-V characteristics of the different cells measured under 1 sun AM 1.5 G standard illumination conditions are reported in Fig. 1b. The results are in line the observation done for the dummy cells, as it is clear how the lower resistivity of the Pt-Ti electrode allowed to obtain a better FF for the full DSSC. Nevertheless, when the treated F-LIG counter electrode was employed, a higher short circuit current density was achieved. For the DSSC that included the treated F-LIG counter a conversion efficiency of 4.17% was achieved which was comparable with the value obtained for the Pt-Ti metallic counter electrode, equal to 4.21%. The other parameters obtained for the DSSC are summarized in Table 1, from which it is clear how the treatment performed on the F-LIG counter electrode drastically improved the performances with respect to the untreated F-LIG electrode, with higher values of both short circuit current density (J_{sc}) and fill factor (FF). Finally, the treated F-LIG electrode also outperformed also the Pt-ITO electrode confirming itself as a cheaper, easy-to-make alternative to Pt-coated flexible counter electrodes for DSSC.

3.2. *Laser-induced graphene as counter electrode for $Cu^{(II/I)}$-based DSSC*

In recent years, the research interest focused on finding alternative redox mediators that would allow to obtain a higher open circuit voltage (V_{oc}). Substantial work has been published regarding cobalt-based electrolytes and how this mediator works in combination with carbon based counter electrodes [57,58]. Much less material has been published regarding the combination of $Cu^{(II/I)}$-based electrolytes and carbon based materials. To the present moment, the best performing combination have been found with electropolymerized PEDOT counter electrodes, where efficiencies of 13% have been reported [9]. For this reason, we decided to investigate the possibility of using LIG electrodes in combination with $Cu^{(II/I)}$-based electrolytes. Here we compared the F-LIG electrodes and flexible ITO/PET electrodes coated with PEDOT (PEDOT-ITO), fabricated as previously reported in literature [24].

Fig. 2 present the comparison between the EIS measurements and the Tafel plot performed on symmetric dummy cells prepared as reported in

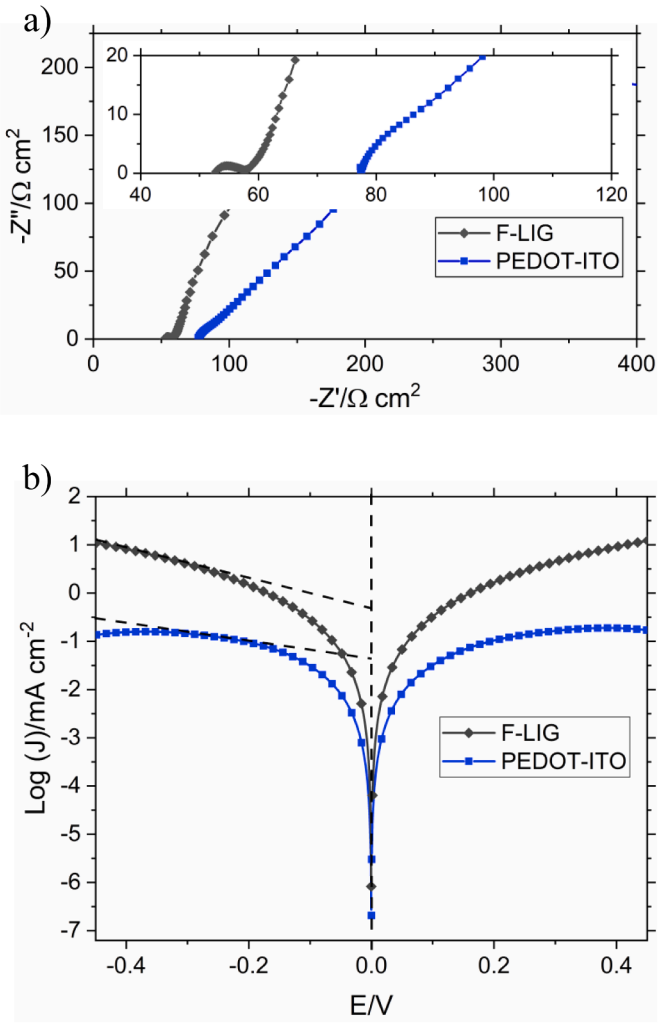

Fig. 2. Comparison of (a) EIS measurements and (b) Tafel polarization of symmetric dummy cell prepared with F-LIG and flexible PEDOT-ITO counter electrodes.

Section 2.3. It must be emphasized the fact that, based on the good performances showed by the untreated F-LIG counter electrode for the $Cu^{(II/I)}$-based electrolyte, here the treatment with AC and CB was avoided with the goal of taking full advantage of the extremely easy one-step fabrication procedure of the F-LIG material. Moreover, as it can be seen from the high frequency region of the Nyquist plot (Fig. 2a), the F-LIG counter electrodes showed a charge transfer resistance of 2.2 Ω cm^2, which was lower that the value obtained for the PEDOT-ITO counter electrode, equal to 7.2 Ω cm^2. Here again the high surface area of the F-LIG electrode seems to play a major role facilitating the reduction of the redox mediator.

In Fig. 3 the field emission scanning electron microscopy (FESEM) images of the two materials show how the F-LIG indeed present its distinctive porous structure already observed in our previous work [45]. Moreover, the graphitic nature of the obtained material was also confirmed performing micro-Raman spectroscopy, and the results are reported in the supplementary material. From this it is evident how the F-LIG electrode will likely provide a high catalytic surface available for the redox reaction, reasonably higher than that provided by the PEDOT-ITO electrode which surface morphology display nonetheless an open mesoporous structure, as already observed in the literature [24]. Moreover, at higher magnification it can be seen that the F-LIG electrodes shows large macro-pores that would allow a better diffusion of the bulky $Cu^{(II/I)}$ redox complex, as previously observed by others [59].

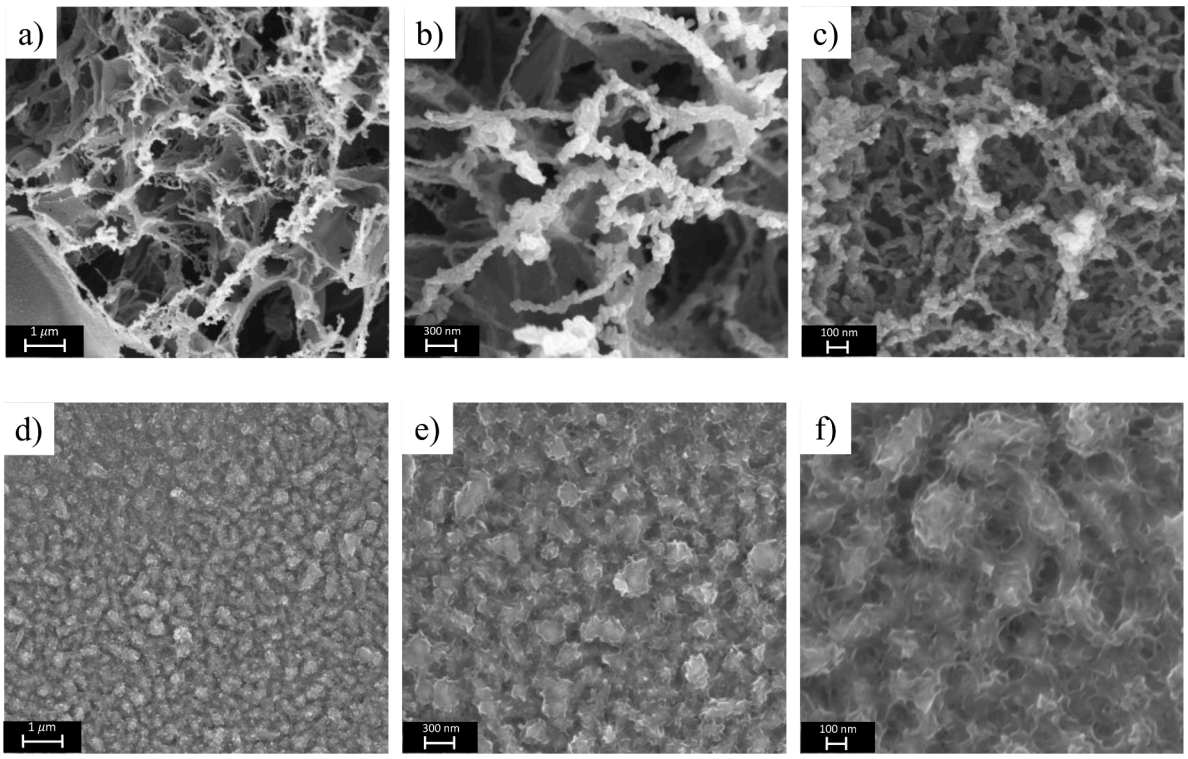

Fig. 3. Field emission scanning electron microscopy of (a-c) F-LIG electrodes (d-f) PEDOT-ITO, presented at different magnifications.

To further investigate the difference between the F-LIG and the PEDOT-ITO electrodes in combination with the $Cu^{(II/I)}$-based mediator, Tafel polarization plots were recorded and reported in Fig. 2b. The Tafel plots, in which the logarithm of the recorded anodic and cathodic currents is reported with respect to the applied voltage, have been exploited in previous works to extract information about the catalytic activity of different counter electrode materials, performing the measurements in symmetrical dummy cells [60,61]. The region at medium overpotential with respect to the equilibrium potential, often found for voltages higher than 120 mV in absolute value, is defined as the Tafel zone. In this zone, the logarithm of the recorded current can be linearly approximated with respect to the applied voltage, and the intercept with the equilibrium potential line can be considered as the exchange current density

$$J_0 = R \times T/(n \times F \times R_{ct}) \quad (1)$$

where n is the number of electrons involved in the reaction, R is the gas constant, T is the temperature, F is the Faraday's constant and R_{ct} is the charge transfer resistance [61].

It must be noted that, besides being largely reported as a technique to evaluate the performances of different materials when employed as counter electrodes for DSSCs, there are some works that highlight how care should be taken when selecting the portion of the Tafel curve to be approximated in order to extract the exchange current [62]. These studies therefore suggest using the derivative of the logarithm of the recorded current to appropriately perform the approximation. By this method, for the PEDOT-ITO materials a J_0 of 0.741 mA cm^{-2} was extrapolated, which correspond to a value of R_{ct} of 2.9 Ω cm^2, according to equation 1. For the F-LIG electrode instead, a J_0 of 0.259 mA cm^{-2} was obtained, corresponding to a value of 8.3 Ω cm^2 for the R_{ct}. The values compare quite successfully with the one extracted from the Nyquist plots.

Furthermore, the electrocatalytic performances of the F-LIG and the PEDOT-ITO electrodes were investigated by cyclic voltammetry (CV) measurements performed in a three-electrode cells. The measurements were performed as reported in the literature, using a 5 mM solution of $Cu^{+}(tmby)_2$ TFSI in 0.1 M LiTFSI/acetonitrile. [63] Ag/AgCl (saturated in LiCl ethanol) was used as a reference electrode and a Pt bar was used as a counter electrode. The geometric area of the tested electrodes was 0.5 cm^2 and the measurements were performed with a scan rate of 10 mV/s. The results are reported in Fig. 4.

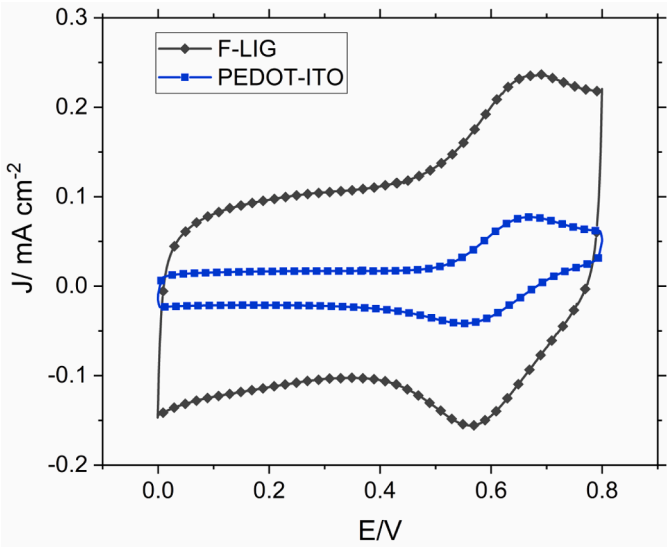

Fig. 4. Comparison of IV characteristic of DSSC fabricated with F-LIG and PEDOT-ITO counter electrode performed under AM 1.5 G illumination and 1000 lux LED indoor illumination.

The CV measurements confirmed once more the higher performance

of the F-LIG electrode with respect to the PEDOT-ITO one. The first feature that can be extracted from these measurements is the voltage separation between the anodic and cathodic reaction peaks, which gives an estimation of the reversibility of the redox reaction. [64] It can be observed that both electrodes show almost identical reversibility, whit peak separation of 0.12 V for F-LIG and PEDOT-ITO electrodes. On the other hand, looking at the peak current density measured for the two electrodes, it can be seen that F-LIG electrodes produced a much higher anodic and cathodic current densities with respect of PEDOT-ITO electrodes. Considering that both electrodes had the same geometric area, this increase can be only ascribed to a higher catalytic activity granted by the F-LIG electrodes. [65,66] As previously commented, this higher electrocatalytic performance is likely related to the much higher surface area provided by the F-LIG electrodes with respect to the PEDTO-ITO ones. These observations confirm how the F-LIG electrode is expected to work as a good material for the reduction of $Cu^{(II/I)}$-based redox mediators for DSSC.

To validate this hypothesis, we tested the counter electrode materials in full DSSC configuration. In Fig. 5a is reported the comparison between the current-voltage characteristics of the F-LIG and PEDOT-ITO based DSSC under AM 1.5 G illumination conditions. It can be seen how the F-LIG based DSSC outperformed its PEDOT based counterpart, with conversion efficiencies of 4.96% and 3.08%, respectively. This difference is mostly related to the much higher J_{sc} generated by the F-LIG based DSSC, which again can be linked to the lower R_{ct} extracted from the EIS measurement of the F-LIG dummy cells. The other main photovoltaic parameters are reported in Table 2 from which it can be seen how the fabricated cells provided similarly high values of V_{oc}, close to 1 V, which confirms one of the advantages of using the $Cu^{(II/I)}$-based redox mediator with respect to other redox couples.

After having recorded the IV characteristics of the different DSSC under standard AM 1.5 G illumination condition we performed the same measurements under artificial light illumination, with an illuminance of 1000 lux, reported in Fig. 5b. It is now widely recognized that one of the main present and future scope of DSSCs is the possibility of harvesting energy from artificial illumination in indoor environments, to be used to power low power electronics such as Internet of Things distributed sensors [67]. In this illumination conditions the combination of low light intensity and better spectral matching between the emission spectrum of indoor lights and the absorption spectrum of sensitizing dyes enables outstanding values of photo-conversion efficiencies [68]. As expected, both cells showed an improvement in performances with a twofold increase in photo-conversion efficiency, as reported in Table 2.

Table 2
Summary of the main parameter extracted from the IV characterization of the full DSSC under AM 1.5 G illumination condition and at 1000 lux LED indoor condition.

Light source	Counter electrode	Jsc (mA cm^{-2})	Voc (V)	FF	η (%)
AM 1.5 G	PEDOT-ITO	5.36	0.98	0.58	3.08
	F-LIG	8.89	0.94	0.59	4.96
1000 lux	PEDOT-ITO	0.045	0.83	0.61	7.77
	F-LIG	0.064	0.82	0.58	9.64

3.3. *Bending stress of F-LIG and PEDOT-ITO flexible counter electrodes*

One of the goals of this work was to show how the F-LIG electrodes could act as a flexible counter electrode for $Cu^{(II/I)}$-based DSSC. To test their flexibility, electrodes with dimension 0.5 × 2 cm were prepared

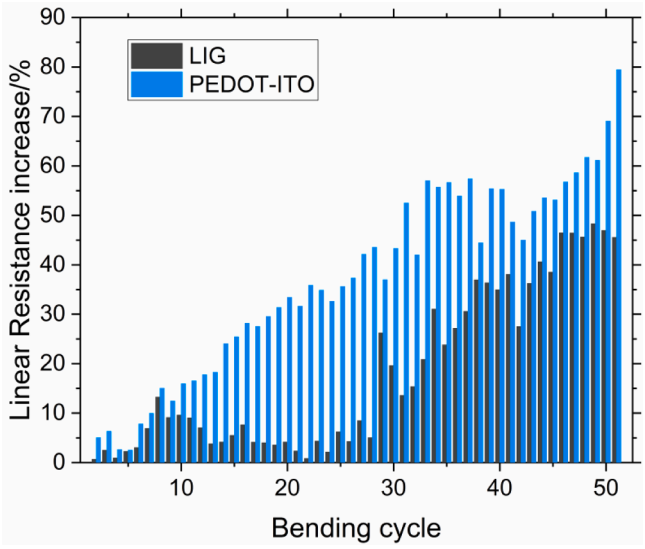

Fig. 6. Variation of linear resistance after multiple bending cycles (bending radius 13 mm) of F-LIG and PEDOT-ITO electrodes.

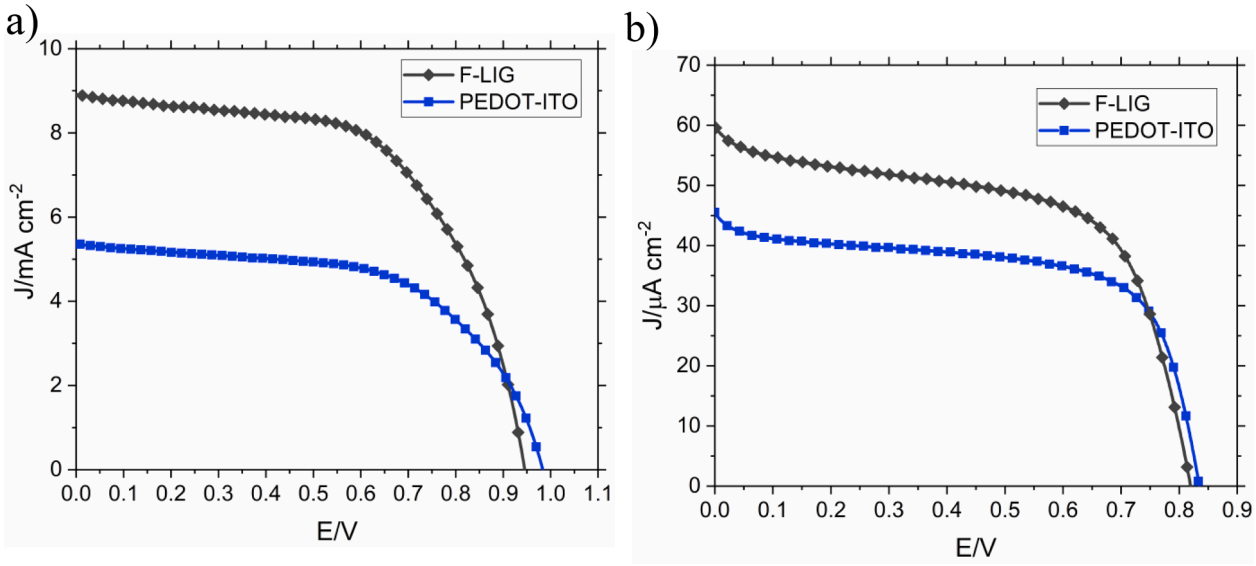

Fig. 5. Comparison of IV characteristic of DSSC fabricated with F-LIG and PEDOT-ITO counter electrode performed under AM 1.5 G illumination and 1000 lux LED indoor illumination.

and were subjected to multiple bending cycles with a bending ratio of 13 mm. After each cycle their linear resistance along the bending direction was recorded. The results are reported in Fig. 6. As it can be seen, the F-LIG electrodes showed a much better stability with respect to the PEDOT-ITO electrodes, with only a 10% increase in linear resistance after the first 30 cycles, lower than the 40% increase recorded for the PEDOT-ITO electrode.

Moreover, it is clear how the ITO-based electrode starts to degrade right from the firsts bending cycles, with an almost linear rise in resistance, which led to a relative increase after 50 bending cycles of around 80%. This value is much lower than the one recorded for the F-LIG equal to 40% at the end of the test. This observation is in line with the finding reported in the literature about the bendability of LIG-based electrodes and devices [69,70]. Furthermore, it is well known how transparent oxides such as ITO deposited on flexible polymeric substrates like PET presents limits from the bendability point of view because of the tendency of the oxide to crack and eventually delaminate from the substrate [71,72].

3.4. Integrated energy harvesting and storage system based on F-LIG electrodes

The starting idea of this work was to verify whether a laser-induced graphene electrode could work as an efficient counter electrode for DSSC, since this finding would enable the possibility of integrating them with a LIG-based supercapacitor, obtaining a self-rechargeable energy harvesting and storage (HS) system. We fabricated such a device in which the two electrodes of the supercapacitor and the counter electrode of the solar cell were fabricated in a single step on the same flexible substrate. The details are provided in Section 2.4 and a picture of the fabricated device is reported in Fig. 7.

First, the harvesting section of the integrated device was characterized under standard AM 1.5 G illumination. The obtained IV curves are reported in Fig. 8a and show how the flexible device show an V_{oc} of 0.92 V, which is allowed by the $Cu^{(II/I)}$-based redox mediator and is in line with the results obtained for the rigid DSSC reported in Section 3.2. Moreover, a high FF of 0.75 was calculated, showing how the low resistance of the Ti grid, used as current collector, allowed to reduce the overall series resistance of the device. On the other hand, such a high FF resulted also from the fact that the flexible cell reported here showed a J_{sc} of 1.2 mA cm^{-2}, which was much lower with respect to the one measured for the rigid devices reported in Section 3.2.

This low value of generated current was most likely connected to the intrinsic configuration of the flexible cell, in which, to avoid the short circuit between the grid-based photoanode and the LIG-based counter electrode, a porous fibreglass separator was used and impregnated with the electrolyte solution. The thickness of the fibreglass separator was equal to 60 μm, to which the thickness of the Ti grid (60 μm) must be added to obtain the actual distance between the counter electrode and the active part of the photoanode, that was therefore higher than 100 μm. It was already observed in other works that the distance between the electrodes is a crucial parameter in DSSC employing $Cu^{(II/I)}$-based electrolytes since these complexes are bulky and suffer in terms of diffusion when the thickness of the electrolyte layer is increased [59]. This was the limitation of the flexible configuration in which the slow diffusion of the redox mediator between the electrodes most likely limited the maximum current that could be generated by the cell.

The device was characterized also under indoor illumination conditions and the IV characteristic is reported in Fig. 8b. The reduce light intensity clearly results in a lower photo-generate current density, which in this case was equal to 17.3 μA cm^{-2}, again lower than the value observed for the rigid DSSC. As always observed for DSSC in the literature, also the V_{oc} was affected by the reduced light intensity [14]. A value of 0.67 V was obtained that will reduce the maximum charging voltage that could be achieved for the HS integrated device under indoor light with respect to the simulated solar illumination conditions.

Even though the flexible configuration reduced the performances of the DSSC with respect to the rigid one, it enabled the ability of the LIG-

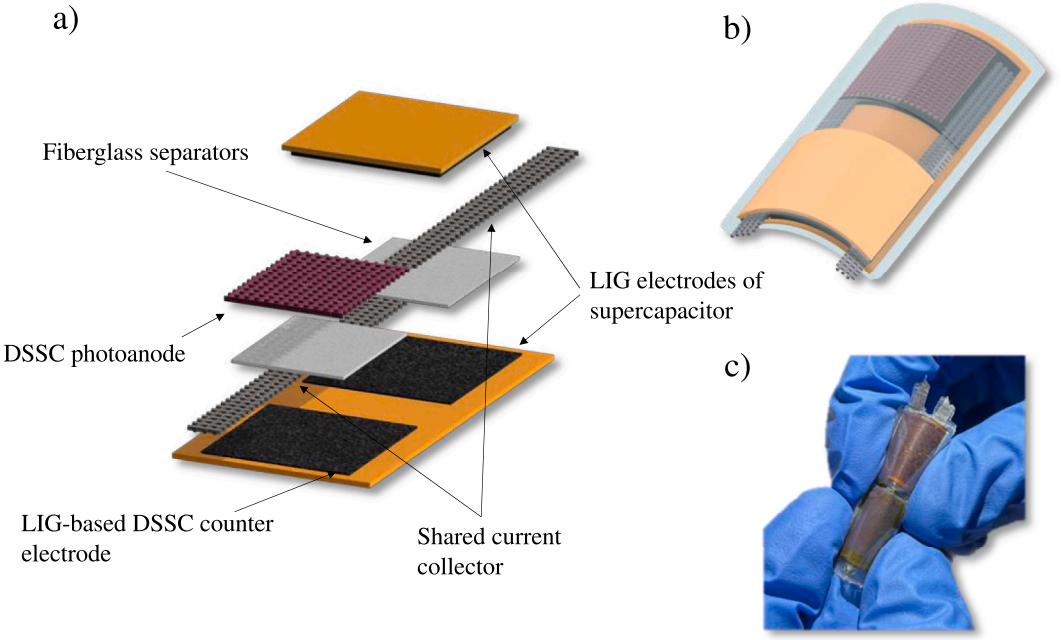

Fig. 7. 3D model of device assembly of the LIG-based integrated energy harvesting and storage systems integrating LIG-based dye-sensitized solar cell and a LIG-based supercapacitor.

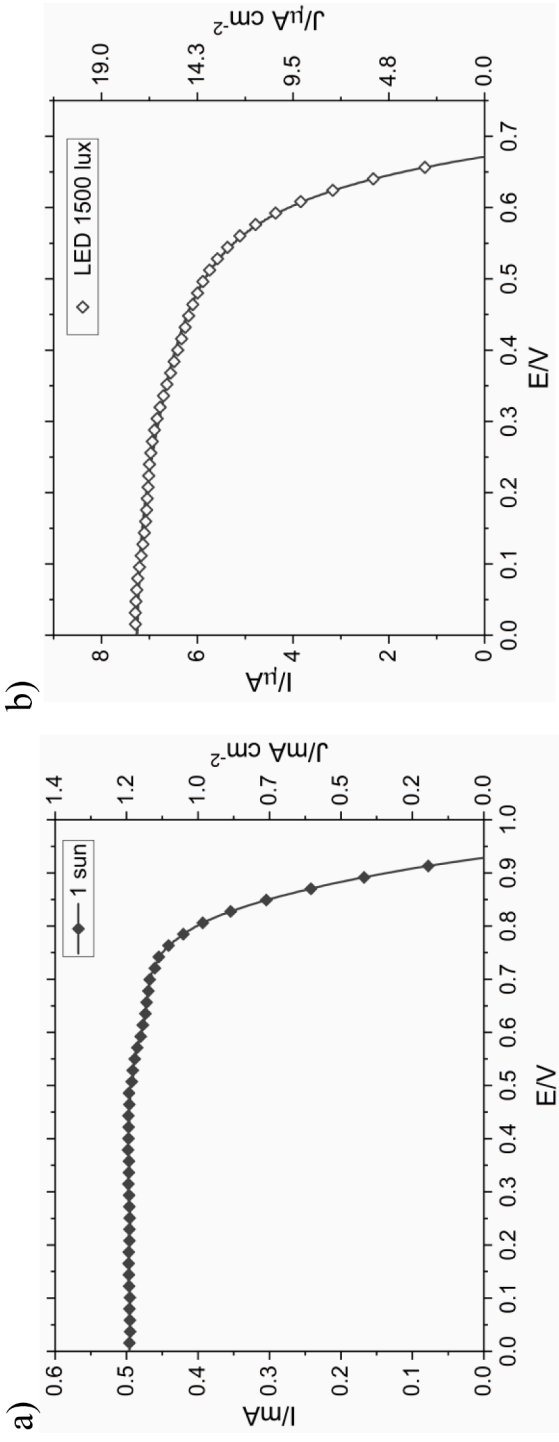

Fig. 8. IV characteristic of flexible LIG-based DSSC under (a) AM 1.5 G illumination condition and (b) 1500 lux indoor LED illumination.

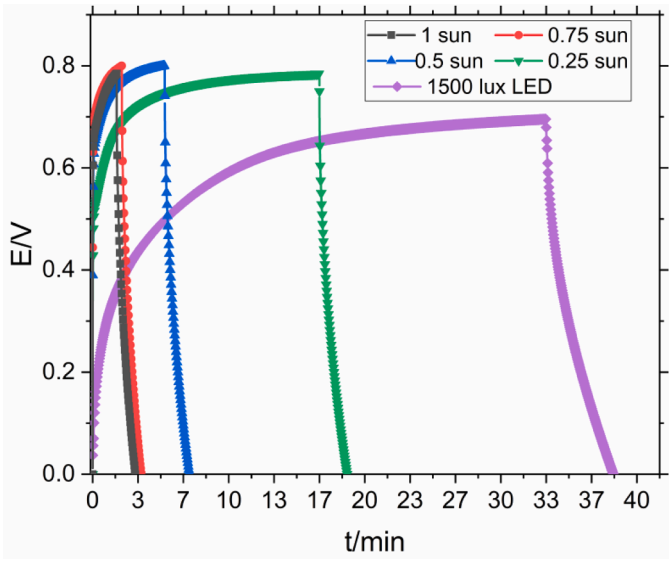

Fig. 9. Photo-charge/discharge measurements performed at different illumination conditions.

based HS integrated device to accumulate energy from natural and artificial light. To demonstrate this, we performed photo-charge/discharge measurements in which, during the first step, the device was illuminated to allow the LIG-based SC to self-charge thanks to the current generated by the LIG-based DSSC, and in a second step the illumination was removed and the device was discharged at a constant current equal to 0.125 mA, corresponding to a current density of 0.4 mA cm^{-2} with respect to the area of the SC. The process was performed in simulated solar illumination, at different light intensities, and under indoor LED light illumination, with an illuminance of 1500 lux. The results are reported in Fig. 9, in which the device voltage is reported with respect to time, and it shows how the device was able to self-charge when placed under illumination. As expected, the maximum charging voltage decreased with reduced light intensity, which is connected to the reduction of the V_{oc} of the DSSC. Nevertheless, under 1 sun illumination, the device was able to self-charge in 1.8 min to the goal voltage, which was set to 0.8 V to avoid degradations in the aqueous-based electrolyte of the SC. As the light intensity was reduced, a plateau in the charging voltage started to appear. As it can be seen, for light intensities lower than 0.5 sun, the desired voltage of 0.8 V became impossible to achieve and a new condition for the interruption of the photo-charging step was needed, so it was decided to consider a variation of the photo-charging voltage lower than 1 μV s^{-1} as the limiting parameter.

From the photo-charge/discharge measurements the storage efficiency (η_S) of the HS device was calculated with the formula $\eta_S = E_{discharge} / E_{photo\text{-}charge}$ where $E_{discharge}$ is the extracted energy, calculated integrating the power extracted during discharge and $E_{photo\text{-}charge}$ is the same energy calculated during photo-charge. The storage efficiency then evaluates how much of the energy generated by the DSSC can be extracted from the SC and is available to power electronic loads such as low-power sensors and IoT devices. This value is reported in comparison with the charging time and the extracted energy at different illumination conditions in Fig. 10.

It is clear how at reduced light intensity, the charging time increases due to lower photo-charging currents generated by the DSSC. Nevertheless, the storage efficiency shows the opposite behaviour, with higher values when the HS device is photo-charged at lower intensities, with values higher than 30%. This evidence could be explained by the fact that charging the supercapacitor at lower currents allows a better and more uniform electrodes charging and consequently, allowing a higher level of energy extracted from the SC at lower light intensities even if the maximum charging voltage decreases.

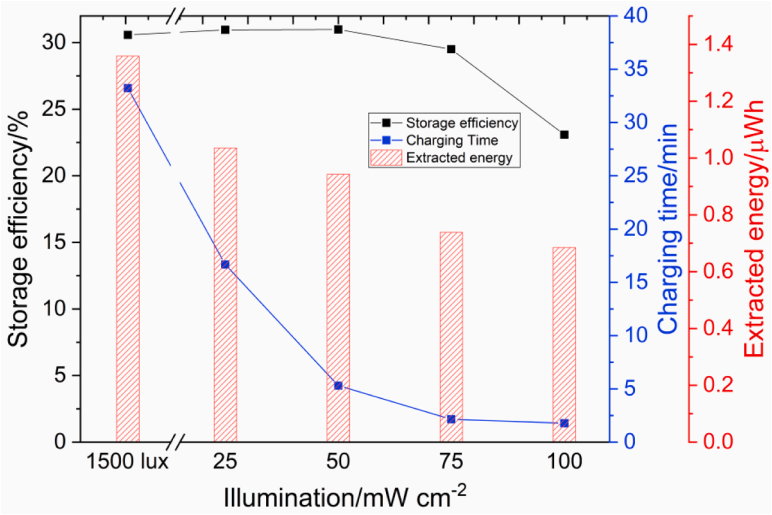

Fig. 10. Comparison between storage efficiency, charging time and extracted energy calculated from photo-charge/discharge measurements reported with respect to illumination conditions.

Conclusions

In this work, we demonstrated that laser-induced graphene (LIG) electrodes directly obtained from polyimide sheets can be used as flexible counter electrodes for DSSC. We showed that, thanks to their high surface area, when used in combination with iodine-based electrolytes, LIG can effectively substitute Pt-coated electrodes. LIG-based electrodes shower a charge transfer resistance (R_{ct}) of 1.3 Ω cm^2 with respect to the value obtained for Pt-coated electrode, equal to 2.3 Ω cm^2. An even lower value, equal to 0.5 Ω cm^2 was obtained when the LIG electrodes were infiltrated with active carbon and carbon black particles. The LIG-based DSSC showed comparable performances with respect to the Pt-based counterpart, with photoconversion efficiencies of 4.17% and 4.21%, respectively.

For the first time, LIG was tested as a catalytic material for the fabrication of counter electrodes in DSSC using $Cu^{(II/I)}(tmby)_2TFSI_{2/1}$ as a redox shuttle. With the $Cu^{(II/I)}$-based electrolyte, the LIG-based electrodes showed a R_{ct} of 2.2 Ω cm^2 with was much lower compared to the one obtained with a PEDOT-coated ITO/PET flexible electrode, equal to 7.2 Ω cm^2. This allowed to reach an open circuit voltage of 0.94 V and a photoconversion efficiency of 4.96% for a LIG-based DSSC, which was 60% more efficient to the one fabricated with the PEDOT-coated ITO/PET electrode.

Moreover, flexible LIG electrodes showed a 45% relative increase in electrical resistance after 50 bending cycles at 13 mm bending ratio, with respect to the value of 80% reached by PEDOT-based flexible electrodes.

Finally, thanks to the one-step laser fabrication process of LIG electrodes, a flexible self-rechargeable energy storage system for indoor applications was demonstrated by integrating a DSSC and a SC in which the counter electrode of the DSSC and the two capacitive electrodes of the SC were made of LIG. The device was able to self-charge when exposed to light, with a storage efficiency that increased at lower illumination intensities, starting from 23% at simulated 1 sun illumination condition and reaching 30% under 1500 lux indoor artificial light illumination. We believe that, with further developments, this device could work as an energy source for self-powered indoor connected IoT devices.

Funding

This research did not receive any specific grant from funding agencies in the public, commercial, or not-for-profit sectors.

CRediT authorship contribution statement

Roberto Speranza: Methodology, Investigation, Writing – original draft, Writing – review & editing, Visualization, Conceptualization. **Marco Reina:** Methodology, Investigation, Writing – review & editing. **Pietro Zaccagnini:** Methodology, Investigation, Validation, Writing – review & editing. **Alessandro Pedico:** Investigation. **Andrea Lamberti:** Conceptualization, Validation, Writing – review & editing, Supervision, Project administration.

Declaration of Competing Interest

The authors declare that they have no known competing financial interests or personal relationships that could have appeared to influence the work reported in this paper.

Supplementary materials

Supplementary material associated with this article can be found, in the online version, at doi:10.1016/j.electacta.2023.142614.

References

[1] A.B. Muñoz-García, et al., Dye-sensitized solar cells strike back, Chem. Soc. Rev. 50 (22) (2021) 12450–12550, https://doi.org/10.1039/D0CS01336F.
[2] T.V. Arjunan, T.S. Senthil, Review: dye sensitised solar cells, Mater. Technol. 28 (1–2) (Mar. 2013) 9–14, https://doi.org/10.1179/1753555712Y.0000000040.
[3] M. Kokkonen, et al., Advanced research trends in dye-sensitized solar cells, J. Mater. Chem. A 9 (17) (2021) 10527–10545, https://doi.org/10.1039/D1TA00690H.
[4] N.I. Mustafa, et al., Environmental performance of window-integrated systems using dye-sensitised solar module technology in Malaysia, Sol. Energy 187 (Jul. 2019) 379–392, https://doi.org/10.1016/j.solener.2019.05.059.
[5] M.L. Parisi, S. Maranghi, R. Basosi, The evolution of the dye sensitized solar cells from Grätzel prototype to up-scaled solar applications: a life cycle assessment approach, Renew. Sustain. Energy Rev. 39 (Nov. 2014) 124–138, https://doi.org/10.1016/j.rser.2014.07.079.
[6] A. Ghosh, Potential of building integrated and attached/applied photovoltaic (BIPV/BAPV) for adaptive less energy-hungry building's skin: a comprehensive review, J. Clean. Prod. 276 (Dec. 2020), 123343, https://doi.org/10.1016/j.jclepro.2020.123343.
[7] A. Ghosh, Fenestration integrated BIPV (FIPV): a review, Sol. Energy 237 (May 2022) 213–230, https://doi.org/10.1016/j.solener.2022.04.013.
[8] P. Selvaraj, A. Ghosh, T.K. Mallick, S. Sundaram, Investigation of semi-transparent dye-sensitized solar cells for fenestration integration, Renew. Energy 141 (2019) 516–525, https://doi.org/10.1016/j.renene.2019.03.146.
[9] D. Zhang, et al., A molecular photosensitizer achieves a Voc of 1.24V enabling highly efficient and stable dye-sensitized solar cells with copper(II/I)-based electrolyte, Nat. Commun. 12 (1) (Mar. 2021) 1777, https://doi.org/10.1038/s41467-021-21945-3.

[10] K. Kakiage, Y. Aoyama, T. Yano, K. Oya, J. Fujisawa, M. Hanaya, Highly-efficient dye-sensitized solar cells with collaborative sensitization by silyl-anchor and carboxy-anchor dyes, Chem. Commun. 51 (88) (2015) 15894–15897, https://doi.org/10.1039/C5CC06759F.

[11] M. Freitag, et al., Copper phenanthroline as a fast and high-performance redox mediator for dye-sensitized solar cells, J. Phys. Chem. C 120 (18) (May 2016) 9595–9603, https://doi.org/10.1021/acs.jpcc.6b01658.

[12] A. Colombo, C. Dragonetti, D. Roberto, F. Fagnani, Copper complexes as alternative redox mediators in dye-sensitized solar cells, Molecules 26 (1) (Jan. 2021) 194, https://doi.org/10.3390/molecules26010194.

[13] M. Freitag, et al., Dye-sensitized solar cells for efficient power generation under ambient lighting, Nat. Photonics 11 (6) (Jun. 2017) 372–378, https://doi.org/10.1038/nphoton.2017.60.

[14] H. Michaels, et al., Dye-sensitized solar cells under ambient light powering machine learning: towards autonomous smart sensors for the internet of things, Chem. Sci. 11 (11) (2020) 2895–2906, https://doi.org/10.1039/C9SC06145B.

[15] H. Elahi, K. Munir, M. Eugeni, S. Atek, P. Gaudenzi, Energy harvesting towards self-powered IoT devices, Energies 13 (21) (Oct. 2020) 5528, https://doi.org/10.3390/en13215528.

[16] "Energy consumption and IoT technologies: what to know," *Information Age*, Oct. 29, 2019. https://www.information-age.com/energy-consumption-and-iot-technologies-what-to-know-123485884/(accessed Mar. 13, 2021).

[17] N.A. Nordin, et al., Integrating photovoltaic (PV) solar cells and supercapacitors for sustainable energy devices: a review, Energies 14 (21) (Nov. 2021) 7211, https://doi.org/10.3390/en14217211.

[18] R. Speranza, P. Zaccagnini, A. Sacco, A. Lamberti, High-voltage energy harvesting and storage system for internet of things indoor application, Sol. RRL (Jul. 2022), 2200245, https://doi.org/10.1002/solr.202200245.

[19] A. Takshi, B. Aljafari, T. Kareri, E. Stefanakos, A critical review on the voltage requirement in hybrid cells with solar energy harvesting and energy storage capability, Batter. Supercaps 4 (2) (Feb. 2021) 252–267, https://doi.org/10.1002/batt.202000223.

[20] N. Vlachopoulos, et al., New approaches in component design for dye-sensitized solar cells, Sustain. Energy Fuels 5 (2) (2021) 367–383, https://doi.org/10.1039/D0SE00596G.

[21] Electro-Materials Research Laboratory, Centre for Nanoscience and Technology, Pondicherry University, Puducherry –605014, India, A Facile Polyvinylpyrrolidone assisted solvothermal synthesis of zinc oxide nanowires and nanoparticles and their influence on the photovoltaic performance of dye sensitized solar cell, ES Energy Environ. (2019), https://doi.org/10.30919/esee8c280.

[22] A. Hagfeldt, G. Boschloo, L. Sun, L. Kloo, H. Pettersson, Dye-sensitized solar cells, Chem. Rev. 110 (11) (Nov. 2010) 6595–6663, https://doi.org/10.1021/cr900356p.

[23] V. Murugadoss, P. Panneerselvam, C. Yan, Z. Guo, S. Angaiah, A simple one-step hydrothermal synthesis of cobalt nickel selenide/graphene nanohybrid as an advanced platinum free counter electrode for dye sensitized solar cell, Electrochim. Acta 312 (Jul. 2019) 157–167, https://doi.org/10.1016/j.electacta.2019.04.142.

[24] H. Ellis, et al., PEDOT counter electrodes for dye-sensitized solar cells prepared by aqueous micellar electrodeposition, Electrochim. Acta 107 (Sep. 2013) 45–51, https://doi.org/10.1016/j.electacta.2013.06.005.

[25] T. Higashino, H. Imahori, Emergence of copper(I/II) complexes as third-generation redox shuttles for dye-sensitized solar cells, ACS Energy Lett. 7 (6) (Jun. 2022) 1926–1938, https://doi.org/10.1021/acsenergylett.2c00716.

[26] H. Khir, et al., Recent advancements and challenges in flexible low temperature dye sensitised solar cells, Sustain. Energy Technol. Assess. 53 (Oct. 2022), 102745, https://doi.org/10.1016/j.seta.2022.102745.

[27] S.G. Hashmi, J. Halme, T. Saukkonen, E.-.L. Rautama, P. Lund, High performance low temperature carbon composite catalysts for flexible dye sensitized solar cells, Phys. Chem. Chem. Phys. 15 (40) (2013) 17689, https://doi.org/10.1039/c3cp52982g.

[28] M.Y.A. Rahman, Review of graphene and its modification as cathode for dye-sensitized solar cells, J. Mater. Sci. Mater. Electron. 32 (19) (Oct. 2021) 23690–23719, https://doi.org/10.1007/s10854-021-06898-z.

[29] Y. Guo, C. Zhang, Y. Chen, Z. Nie, Research progress on the preparation and applications of laser-induced graphene technology, Nanomaterials 12 (14) (Jul. 2022) 2336, https://doi.org/10.3390/nano12142336.

[30] P. Zaccagnini, D. di Giovanni, M.G. Gomez, S. Passerini, A. Varzi, A. Lamberti, Flexible and high temperature supercapacitor based on laser-induced graphene electrodes and ionic liquid electrolyte, a de-rated voltage analysis, Electrochim. Acta 357 (Oct. 2020), 136838, https://doi.org/10.1016/j.electacta.2020.136838.

[31] F.M. Vivaldi, et al., Three-dimensional (3D) laser-induced graphene: structure, properties, and application to chemical sensing, ACS Appl. Mater. Interfaces 13 (26) (Jul. 2021) 30245–30260, https://doi.org/10.1021/acsami.1c05614.

[32] E. Alhajji, F. Zhang, H.N. Alshareef, Status and prospects of laser-induced graphene for battery applications, Energy Technol. 9 (10) (Oct. 2021), 2100454, https://doi.org/10.1002/ente.202100454.

[33] W. Ma, J. Zhu, Z. Wang, W. Song, G. Cao, Recent advances in preparation and application of laser-induced graphene in energy storage devices, Mater. Today Energy 18 (Dec. 2020), 100569, https://doi.org/10.1016/j.mtener.2020.100569.

[34] M. Parmeggiani, et al., Laser-induced graphenization of textile yarn for wearable electronics application, Smart Mater. Struct. 30 (10) (Oct. 2021), 105007, https://doi.org/10.1088/1361-665X/ac182c.

[35] L. Huang, J. Su, Y. Song, R. Ye, Laser-induced graphene: en route to smart sensing, Nano-Micro Lett. 12 (1) (Dec. 2020) 157, https://doi.org/10.1007/s40820-020-00496-0.

[36] M. Ren, J. Zhang, J.M. Tour, Laser-induced graphene synthesis of Co3O4 in graphene for oxygen electrocatalysis and metal-air batteries, Carbon N Y 139 (Nov. 2018) 880–887, https://doi.org/10.1016/j.carbon.2018.07.051.

[37] J. Zhang, M. Ren, Y. Li, J.M. Tour, In situ synthesis of efficient water oxidation catalysts in laser-induced graphene, ACS Energy Lett. 3 (3) (Mar. 2018) 677–683, https://doi.org/10.1021/acsenergylett.8b00042.

[38] P. Zaccagnini, A. Lamberti, A perspective on laser-induced graphene for micro-supercapacitor application, Appl. Phys. Lett. 120 (10) (Mar. 2022), 100501, https://doi.org/10.1063/5.0078707.

[39] L. Andrea, et al., New insights on laser-induced graphene electrodes for flexible supercapacitors: tunable morphology and physical properties, Nanotechnology 28 (17) (2017), 174002–174002.

[40] H. Renuka, P.K. Enaganti, S. Kundu, S. Goel, Laser-induced graphene electrode based flexible heterojunction photovoltaic cells, Microelectron. Eng. 251 (Jan. 2022), 111673, https://doi.org/10.1016/j.mee.2021.111673.

[41] Z. Chu, Y. Wang, L. Jiao, X. Zhang, Laser-scribed reduced graphene oxide as counter electrode for dye-sensitized solar cell, Fuller. Nanotub. Carbon Nanostruct. 27 (12) (Dec. 2019) 914–919, https://doi.org/10.1080/1536383X.2019.1660648.

[42] Z. Chu, L. Jiao, X. Zhang, C. Liu, Facile fabrication of reduced graphene oxide counter electrodes by laser engraver for dye-sensitized solar cell applications, Fuller. Nanotub. Carbon Nanostruct. 29 (2) (Feb. 2021) 100–106, https://doi.org/10.1080/1536383X.2020.1813721.

[43] D.N. Sangeetha, et al., Conductivity/electrochemical study of polyvinyl pyrrolidone-poly(vinyl alcohol)/I3− thin film electrolyte for integrated dye-sensitized solar cells and supercapacitors, J. Electron. Mater. 49 (11) (Nov. 2020) 6325–6335, https://doi.org/10.1007/s11664-020-08432-z.

[44] A. Lamberti, et al., New insights on laser-induced graphene electrodes for flexible supercapacitors: tunable morphology and physical properties, Nanotechnology 28 (17) (Apr. 2017), 174002, https://doi.org/10.1088/1361-6528/aa6615.

[45] M. Reina, et al., Boosting electric double layer capacitance in laser-induced graphene-based supercapacitors, Adv. Sustain. Syst. 6 (1) (Jan. 2022), 2100228, https://doi.org/10.1002/adsu.202100228.

[46] A. Scalia, et al., High energy and high voltage integrated photo-electrochemical double layer capacitor, Sustain. Energy Fuels 2 (5) (2018) 968–977, https://doi.org/10.1039/C8SE00003D.

[47] L.-.Y. Lin, C.-.P. Lee, R. Vittal, K.-.C. Ho, Selective conditions for the fabrication of a flexible dye-sensitized solar cell with Ti/TiO2 photoanode, J. Power Sources 195 (13) (Jul. 2010) 4344–4349, https://doi.org/10.1016/j.jpowsour.2010.01.031.

[48] C. Wu, B. Chen, X. Zheng, S. Priya, Scaling of the flexible dye sensitized solar cell module, Sol. Energy Mater. Sol. Cells 157 (2016) 438–446, https://doi.org/10.1016/j.solmat.2016.07.021.

[49] A. Khan, Y.-.T. Huang, T. Miyasaka, M. Ikegami, S.-.P. Feng, W.-.D. Li, Solution-processed transparent nickel-mesh counter electrode with in-situ electrodeposited platinum nanoparticles for full-plastic bifacial dye-sensitized solar cells, ACS Appl. Mater. Interfaces 9 (9) (Mar. 2017) 8083–8091, https://doi.org/10.1021/acsami.6b14861.

[50] A. Sacco, et al., A long-term analysis of Pt counter electrodes for Dye-sensitized Solar Cells exploiting a microfluidic housing system, Mater. Chem. Phys. 161 (Jul. 2015) 74–83, https://doi.org/10.1016/j.matchemphys.2015.05.013.

[51] R. Kern, R. Sastrawan, J. Ferber, R. Stangl, J. Luther, Modeling and interpretation of electrical impedance spectra of dye solar cells operated under open-circuit conditions, Electrochim. Acta 47 (26) (Oct. 2002) 4213–4225, https://doi.org/10.1016/S0013-4686(02)00444-9.

[52] A. Sacco, Electrochemical impedance spectroscopy: fundamentals and application in dye-sensitized solar cells, Renew. Sustain. Energy Rev. 79 (Nov. 2017) 814–829, https://doi.org/10.1016/j.rser.2017.05.159.

[53] J. Chen, et al., A flexible carbon counter electrode for dye-sensitized solar cells, Carbon N Y 47 (11) (Sep. 2009) 2704–2708, https://doi.org/10.1016/j.carbon.2009.05.028.

[54] A.K.K. Kyaw, et al., Dye-sensitized solar cell with a pair of carbon-based electrodes, J. Phys. Appl. Phys. 45 (16) (Apr. 2012), 165103, https://doi.org/10.1088/0022-3727/45/16/165103.

[55] Y. Wang, M. Wu, X. Lin, Z. Shi, A. Hagfeldt, T. Ma, Several highly efficient catalysts for Pt-free and FTO-free counter electrodes of dye -sensitized solar cells, J. Mater. Chem. 22 (9) (2012) 4009–4014, https://doi.org/10.1039/C2JM15182K.

[56] A. Kaniyoor, S. Ramaprabhu, Thermally exfoliated graphene based counter electrode for low cost dye sensitized solar cells, J. Appl. Phys. 109 (12) (Jun. 2011), 124308, https://doi.org/10.1063/1.3600231.

[57] I.-.P. Liu, Y.-.C. Hou, C.-.W. Li, Y.-.L. Lee, Highly electrocatalytic counter electrodes based on carbon black for cobalt(III)/(II)-mediated dye-sensitized solar cells, J. Mater. Chem. A 5 (1) (2017) 240–249, https://doi.org/10.1039/C6TA08818J.

[58] J. Wu, et al., Counter electrodes in dye-sensitized solar cells, Chem. Soc. Rev. 46 (19) (2017) 5975–6023, https://doi.org/10.1039/C6CS00752J.

[59] S.G. Hashmi, G.G. Sonai, H. Iftikhar, P.D. Lund, A.F. Nogueira, Printed single-walled carbon-nanotubes-based counter electrodes for dye-sensitized solar cells with copper-based redox mediators, Semicond. Sci. Technol. 34 (10) (Oct. 2019), 105001, https://doi.org/10.1088/1361-6641/ab39f0.

[60] M. Wang, et al., CoS supersedes pt as efficient electrocatalyst for triiodide reduction in dye-sensitized solar cells, J. Am. Chem. Soc. 131 (44) (Nov. 2009) 15976–15977, https://doi.org/10.1021/ja905970y.

[61] M. Wu, et al., Economical Pt-free catalysts for counter electrodes of dye-sensitized solar cells, J. Am. Chem. Soc. 134 (7) (Feb. 2012) 3419–3428, https://doi.org/10.1021/ja209657v.

[62] M. Corva, N. Blanc, C.J. Bondue, K. Tschulik, Differential tafel analysis: a quick and robust tool to inspect and benchmark charge transfer in electrocatalysis, ACS Catal. 12 (21) (Nov. 2022) 13805–13812, https://doi.org/10.1021/acscatal.2c03581.

[63] Y. Saygili, et al., Copper bipyridyl redox mediators for dye-sensitized solar cells with high photovoltage, J. Am. Chem. Soc. 138 (45) (Nov. 2016) 15087–15096, https://doi.org/10.1021/jacs.6b10721.
[64] V. Murugadoss, et al., Optimizing graphene content in a NiSe/graphene nanohybrid counter electrode to enhance the photovoltaic performance of dye-sensitized solar cells, Nanoscale 11 (38) (2019) 17579–17589, https://doi.org/10.1039/C9NR07060E.
[65] S.Elindjeane Sheela, V. Murugadoss, R. Sittaramane, S. Angaiah, Development of tungsten diselenide/polyaniline composite nanofibers as an efficient electrocatalytic counter electrode material for dye-sensitized solar cell, Sol. Energy 209 (Oct. 2020) 538–546, https://doi.org/10.1016/j.solener.2020.09.030.
[66] E.S. Sowbakkiyavathi, V. Murugadoss, R. Sittaramane, R. Dhanusuraman, S. Angaiah, Cobalt selenide decorated polyaniline composite nanofibers as a newer counter electrode for dye-sensitized solar cell, Polym. Adv. Technol. 32 (8) (Aug. 2021) 3137–3149, https://doi.org/10.1002/pat.5326.
[67] A. Aslam, et al., Dye-sensitized solar cells (DSSCs) as a potential photovoltaic technology for the self-powered internet of things (IoTs) applications, Sol. Energy 207 (Sep. 2020) 874–892, https://doi.org/10.1016/j.solener.2020.07.029.
[68] M.A. Saeed, K. Yoo, H.C. Kang, J.W. Shim, J.-.J. Lee, Recent developments in dye-sensitized photovoltaic cells under ambient illumination, Dyes Pigm. 194 (Oct. 2021), 109626, https://doi.org/10.1016/j.dyepig.2021.109626.
[69] Z. Peng, et al., Flexible boron-doped laser-induced graphene microsupercapacitors, ACS Nano 9 (6) (Jun. 2015) 5868–5875, https://doi.org/10.1021/acsnano.5b00436.
[70] Z. Peng, J. Lin, R. Ye, E.L.G. Samuel, J.M. Tour, Flexible and stackable laser-induced graphene supercapacitors, ACS Appl. Mater. Interfaces 7 (5) (Feb. 2015) 3414–3419, https://doi.org/10.1021/am509065d.
[71] Y.F. Lan, W.C. Peng, Y.H. Lo, J.L. He, Durability under mechanical bending of the indium tin oxide films deposited on polymer substrate by thermionically enhanced sputtering, Org. Electron. 11 (4) (Apr. 2010) 670–676, https://doi.org/10.1016/j.orgel.2010.01.008.
[72] M. Nasr Saleh, G. Lubineau, Understanding the mechanisms that change the conductivity of damaged ITO-coated polymeric films: a micro-mechanical investigation, Sol. Energy Mater. Sol. Cells 130 (Nov. 2014) 199–207, https://doi.org/10.1016/j.solmat.2014.07.011.